

JAAS

Accepted Manuscript



This is an *Accepted Manuscript*, which has been through the Royal Society of Chemistry peer review process and has been accepted for publication.

Accepted Manuscripts are published online shortly after acceptance, before technical editing, formatting and proof reading. Using this free service, authors can make their results available to the community, in citable form, before we publish the edited article. We will replace this *Accepted Manuscript* with the edited and formatted *Advance Article* as soon as it is available.

You can find more information about *Accepted Manuscripts* in the [Information for Authors](#).

Please note that technical editing may introduce minor changes to the text and/or graphics, which may alter content. The journal's standard [Terms & Conditions](#) and the [Ethical guidelines](#) still apply. In no event shall the Royal Society of Chemistry be held responsible for any errors or omissions in this *Accepted Manuscript* or any consequences arising from the use of any information it contains.

On the performance of laser-induced breakdown spectroscopy for quantitative analysis of minor and trace elements in glass

Erwan Negre,^{a,b} Vincent Motto-Ros,^a Frederic Pelascini,^b Sandrine Lauper,^c Danielle Denis,^c and Jin Yu^{a*}

^a*Institut Lumière Matière, UMR5306 Université Lyon 1-CNRS, Université de Lyon, 69622 Villeurbanne cedex, France*

^b*CRITT Matériaux Alsace, 19, rue de St Junien 67305 Schiltigheim, France*

^c*Institut National de Police Scientifique, 31 av. Franklin Roosevelt, 69134 Ecully, France*

Abstract

The analytical figures of merit of laser-induced breakdown spectroscopy (LIBS) for elemental analysis of glass have been evaluated using a laboratory prototype of LIBS instrument for the quantification of 4 elements, Ti, Cr, Ca and Ba. Two sets of samples were prepared or collected for the assessment. The first one consisted of 10 laboratory-prepared fused beads with the elemental content determined by X-ray fluorescence (XRF), an established analytical technique which was considered in our study as the reference technique for the assessment of the LIBS technique. Among them, 8 were used as reference samples and 2 as “unknown” samples for test. The calibration curves were thus established with the references. And the counter calibration led to the determination of the elemental content in the unknown samples. Such calibration procedure allowed assessing the figures of merit of LIBS together with the used setup and measurement protocol about a certain number of key parameters, such as the correlation to a linear regression of the calibration data, limit of detection (LoD), repeatability, reproducibility and relative accuracy. The second set of samples was collected from different origins and consisted of 8 bottle glass fragments, which were different in appearance (color, surface) and in content for the 4 analyzed elements. Their elemental concentrations were first determined using XRF. The LIBS calibration curves established with the fused beads were thus used to perform the analysis of 2 glass

* Corresponding author. E-mail address: jin.yu@univ-lyon1.fr (Jin Yu).

1 fragments with elemental contents lying around the range of the calibration concentration.
2
3 The further analysis of the ensemble of glass fragments allowed assessing the matrix effect
4
5 introduced by the different types of glasses and extending the calibration curves over a very
6
7 large concentration range from several ppm to several percent. We show that the self-
8
9 absorption effect observed over such large concentration range can be taken into account by
10
11 using a quadratic regression.

12 **Keywords:**

13
14
15 Laser-induced breakdown spectroscopy, Glass, Analytical figures of merit
16
17
18
19

20 **1. Introduction**

21
22 Glass composition can be very different according to the type of glass (soda-lime glass,
23
24 borosilicate glass, fused silica ...), the application purpose, and the manufacturing process.¹
25
26 Minor or trace elements can be added in the fabrication process to obtain specific properties
27
28 whether physical, optical, electrical, mechanical or thermal, for example lead for brilliance
29
30 and weight; boron for thermal and electrical resistance; barium to increase the refractive index
31
32 for optical glass; cerium to absorb infrared rays; metallic oxides to impart color; and
33
34 manganese for decolorizing.² Quantitative elemental analysis of glass represents therefore an
35
36 important issue in glass manufacture industry. Such analysis is also required by a wide range
37
38 of societally important applications. Ancient glasses from archeological sites or historical
39
40 buildings, artwork objects, utensils, or stained glass windows, are analyzed for the
41
42 understanding of their corrosion mechanisms and helping their preservation and restoration.³⁻⁷
43
44 More recently, some works have been also devoted to elemental analysis of nuclear waste
45
46 storage glasses and gotten promising results.⁸

47
48 An important application of elemental analysis of glasses has been found in forensic
49
50 science. Several analytical techniques have been usually used for such analysis, including
51
52 scanning electron microscopy/energy-dispersive X-ray spectroscopy (SEM/EDS), electron
53
54 probe microanalyzer (EPMA), X-ray fluorescence spectrometry (XRF), inductively coupled
55
56 plasma optical emission (or mass) spectrometry (ICP-OES or ICP-MS), or laser ablation
57
58 inductively coupled plasma optical emission (or mass) spectrometry (LA-ICP-OES or LA-
59
60 ICP-MS). Among the above mentioned established analytical techniques, ICP-OES (or MS),
and LA-ICP-OES (or MS) are those who provide the best performance to fit the requirement
of the elemental analysis for forensic science.⁹ Such requirement can be in general expressed

1
2 in terms of limit of detection (LoD), precision, accuracy, discrimination power, sample
3 consumption, time of analysis, ease of use and cost. Even though ICP or LA-ICP provides
4 excellent analytical performance in terms of LoD, precision and accuracy, they are in general
5 time-consuming, destructive for the sample, complicated to use (sample preparation) and
6 quite expansive for the equipment.
7
8
9

10 Recently, laser-induced breakdown spectroscopy (LIBS) has been introduced to provide
11 elemental analysis of glass for various applications and especially for forensic science.^{3-6,8,10-13}
12 With respect to the established techniques, LIBS is expected to provide faster and direct
13 analyses without sample preparation and with almost no sample destruction, as well as easy-
14 to-use and cost-effective instruments. Its ability to provide quantitative analysis of elemental
15 content in various samples has been largely demonstrated. Beside the classical determination
16 method with reference samples and calibration curves, calibration free approach¹⁴ has also
17 been introduced and recently applied to quantitative analysis of glasses.¹⁵ However compared
18 to the ICP-based techniques, LIBS shows today in general quite limited performances not
19 only in terms of LoD, but also in terms of precision, reproducibility and accuracy. Further
20 development efforts are still needed to optimize the LIBS instrumentation and the
21 experimental protocol in order to improve the quantitative analysis ability of the technique.
22 The purpose of the present work is therefore to evaluate the performance of LIBS for
23 quantitative analysis of minor and trace elements in glass with a laboratory prototype of LIBS
24 instrument in which the laser ablation and the plasma emission detection are performed under
25 tight controls with motorized positioning mechanics and computer-assisted monitoring and
26 diagnostics.¹⁶ For such purpose, two sets of samples were analyzed. The first set consisted of
27 fused beads prepared in laboratory in which minor and trace elements were uniformly
28 distributed in an identical glass matrix. The second set corresponded to collected fragments of
29 bottle glass with different aspects (color, surface) in which a significant space inhomogeneity
30 of the contained elements could be expected. The quantitative analysis performance allowed
31 by the prototype of LIBS instrument together with the associated measurement protocol has
32 been thus evaluated for these two sets of samples. The reference analytical technique used for
33 such evaluation was XRF. Beside the fact that it represents a mature technique usually used
34 for glass analysis, the choice was also motivated by the high performance of this technique
35 demonstrated for discrimination of automotive glass.¹³
36
37
38
39
40
41
42
43
44
45
46
47
48
49
50
51
52
53
54
55
56
57
58
59
60

2. Experimental

2.1. Sample preparation and characterization

Two collections of samples were used in this experiment. The first one was a set of 10 lithium borate samples prepared and characterized by CRITT Matériaux Alsace (<http://www.critt.fr/>) with the technique of fused bead. This technique is known as able to provide samples with good homogeneity. The second one was a set of 8 fragments of bottle glass collected from different origins. These samples presented different visual aspects (color and surface) which may correspond to different matrix effects, and possible space inhomogeneity of the elements to be analyzed. Four elements, Ti, Cr, Ca and Ba were chosen to be analyzed in this work, because they are representatives of elements frequently found in glass (one minor, Ca, and three trace, Ti, Cr and Ba, elements). The concentration of these elements was determined by using XRF (S4 Pioneer, Bruker AXS GmbH) for all the beads and glass fragments. We consider in this work, the concentrations determined by XRF as the reference values for the establishment of LIBS calibration curves and for the assessment of the relative accuracy of LIBS measurements. In such way, the agreement between LIBS and XRF for the different parameters characterizing the figures of merit of an analytical technique will constitute the basis of the assessment intended in this work. The concentrations of the 4 elements of interest determined by XRF for all the samples analyzed in this work are listed in Table 1. We remark here that glass standard reference materials, NIST SRM for example, could also be used in this work. However we have preferred to use the laboratory prepared and characterized samples to better compare, under the similar laboratory operation condition, the two involved analytical techniques, XRF and LIBS. In order to eliminate surface contamination, prior to each analysis, the surface of the samples was cleaned using ethanol.

Table 1 Concentrations of the 4 elements of interest expressed in ppm of weight for the prepared fused beads and the collected bottle glass fragments determined using XRF.

Sample type	Sample name	Concentrations (ppm of weight)			
		Ti	Cr	Ca	Ba
Fused beads as references	FB1	45	223	12613	53
	FB2	32	160	8983	39
	FB3	17	81	4324	19
	FB4	9.0	42	2124	10
	FB5	4.0	18	891	4.0
	FB6	3.0	10	436	3.0
	FB7	2.0	7.0	274	2.0
	FB8	1.0	4.0	100	1.0
Fused beads as unknowns	FB9	14	28	9160	10
	FB10	7.0	7.0	4319	5.0
Collected bottle glass fragments	BG1	2300	470	32380	260
	BG2	60	223	29543	53
	BG3	137	42	23275	120
	BG4	83	750	13170	1050
	BG5	820	81.0	12613	-
	BG6	45	1100	2124	530
	BG7	-	-	434	300
	BG8	280	1450	-	10.0

2.2. Experimental setup

A detailed description of the used experimental setup can be found elsewhere.¹⁶ Laser pulses of the forth harmonic of Q-switched Nd:YAG laser (266 nm, 6 mJ, 5 ns, 10 Hz) were used for ablation. The ablation took place in the atmospheric air. The laser pulse injection and focusing line of the setup is more specifically shown in Fig. 1. The pulses passed through the injection line composed of a pair of lenses (L_1 and L_2) with focal distance of respectively -50 mm and 100 mm. The nearly afocal arrangement of the lens pair expanded the input beam before its final focusing around the sample surface by a third lens of 75 mm focal length (L_3). All the 3 lenses were made in quartz. In particular, the L_1 was mounted on a motorized translation stage, allowing a precise adjustment of the position of the focal point with respect to the sample surface. In our experiment, the laser beam was focused 600 μm under the sample surface with an accuracy of 10 μm . Such shift was necessary to avoid direct breakdown in air and led to the production of a stable plasma.¹⁶ During the measurements, the distance between the sample surface and the lens L_3 was kept constant and monitored by means of a trigonometric surface positioning system involving a laser pointer equipped with a

1
2
3
4
5
6
7
8
9
10
11
12
13
14
15
16
17
18
19
20
21
22
23
24
25
26
27
28
29
30
31
32
33
34
35
36
37
38
39
40
41
42
43
44
45
46
47
48
49
50
51
52
53
54
55
56
57
58
59
60

diffractive output coupler (Z-LASER, ZM18B with cross uniform lines output) which emitted a beam in oblique incidence on the sample surface, and a CCD camera (C_2 in Fig. 1a) which looked at the pattern of the laser pointer on the sample surface as shown in Fig. 1b (red cross). When the sample surface was precisely set to a correct distance with respect to the lens L_3 , one of the orthogonal lines of the laser pointer pattern on the sample surface became superimposed to a reference line fixed in the frame of the camera C_2 as shown in Fig. 1b. During a measurement, if a change of the sample height occurred, an automatic correction was applied to the sample holder to maintain the distance between the lens L_3 and the sample surface.

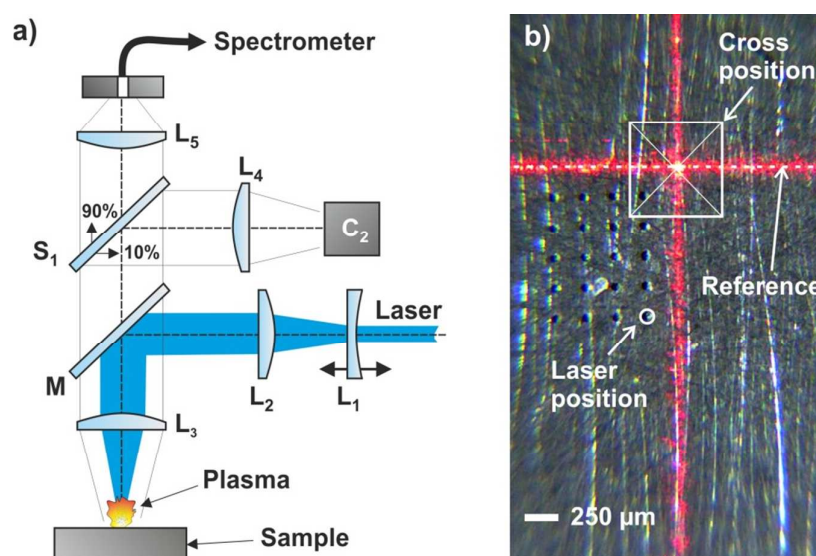


Fig. 1 Schematic representation of the laser injection line and the axial detection line.

The axial detection line was used to collect the emission from the plasma into an optical fiber as shown in Fig. 1a. The plasma emission was first collimated by the lens L_3 . It transmitted through the dielectric mirror M with high reflection at 266 nm and high transmission for wavelengths above 300 nm. The transmitted plasma emission and the scattered visible lights from the sample surface were then separated by a beam splitter S_1 . 10% of these lights were oriented to a CCD camera (C_2) through a lens of 50 mm focal length L_4 , which allowed the last forming an image of the sample surface on the camera C_2 . The remaining part of 90% of the lights was sent to the lens L_5 (focal length $f_5=35$ mm) which focused the plasma emission into an optical fiber connected to a spectrometer. The optical fiber consisted in a bundle of 19 fibers of 100 μm of core diameter assembled in a circular section at its entrance and becoming a linear array at its output end connected to the entrance

1 slit of the spectrometer. A Czerny-Turner spectrometer (Shamrock, Andor Technology) was
2 used with a 1200 l/mm grating. Its spectral resolution was 0.1 nm at 500 nm. The output of
3 the spectrometer was connected to an ICCD camera (iStar Andor Technology).
4
5
6

7 **2.3. Experimental protocol**

8
9 In the experiment, each spectrum was accumulated over 10 laser shots on a same crater. One
10 hundred measurement replicates were performed for each sample with 100 craters distributed
11 on a matrix of 10 craters by 10. The time for such measurement was about two minutes for a
12 sample. The crater diameter and depth were measured to be respectively (140 ± 3) μm and $(35$
13 $\pm 2)$ μm using an optical microscope with the z-stack option (Axio Imager.M2, Carl Zeiss).
14 The crater to crater distance was set to 200 μm . The ablation laser pulse energy was set to a
15 mean value of 6.0 mJ with a standard deviation of 0.15 mJ using a computer-controlled
16 attenuator (ATT266, Quantum Composers). The pulse energy was monitored during the
17 measurements using a power meter with a pulse to pulse response. The ICCD camera for the
18 plasma emission detection was synchronized to laser shots using the trigger signals from a
19 photodiode. The delay and the gate width applied to the ICCD were respectively 0.9 μs and
20 2.0 μs after the laser pulse impact on the sample surface. They were optimized for the used
21 experimental configuration.
22
23
24
25
26
27
28
29
30

31 **2.4. Spectral line selection and line intensity calculation**

32 For high quality quantitative analysis, spectral line selection is a crucial step. A practical
33 constraint in our experiment was that we used a spectrometer with a limited spectral range of
34 about 30 nm in the near UV. Four relatively intense and well resolved lines respectively for
35 the 4 elements of interest were thus selected in 2 spectral windows from 330 nm to 360 nm
36 and from 435 nm to 460 nm. As shown in Fig. 2, the first spectral window covers a line of Ti
37 (Ti II 334.9 nm) and a line of Cr (Cr I 357.9 nm). The second includes a line of Ca (Ca I
38 445.6 nm) and a line of Ba (Ba II 455.4 nm). We can see that all these lines are well isolated
39 and free of spectral interference with respect to other elements (but possibly containing
40 several non-resolved lines of the same element). We checked then eventual self-absorption
41 effect on these lines. The Ti II 334.9 nm line and the Ca I 445.6 nm lines are not resonant
42 lines.¹⁷ The probability for them to be affected by self-absorption is thus small. The Cr I 357.9
43 nm line and the Ba II 455.4 line are however both resonant lines. We checked carefully their
44 state of self-absorption by first looking at the profile of the spectral line and later when the
45 calibration curves will be plotted, the linearity of the curves in order to be sure that the effect
46 of self-absorption is negligible for these lines over the investigated range of concentration. In
47
48
49
50
51
52
53
54
55
56
57
58
59
60

order to establish the calibration curves for the 4 elements of interest, the emission intensities of the 4 chosen lines for a given sample were extracted from the spectra taken in the two spectral ranges by fitting the spectral lines with polynomial function after the baseline being subtracted. The maximum of the fitting function was thus considered as the intensity of the emission line. The extracted intensity was then plotted as a function of the elemental content of the sample determined with XRF.

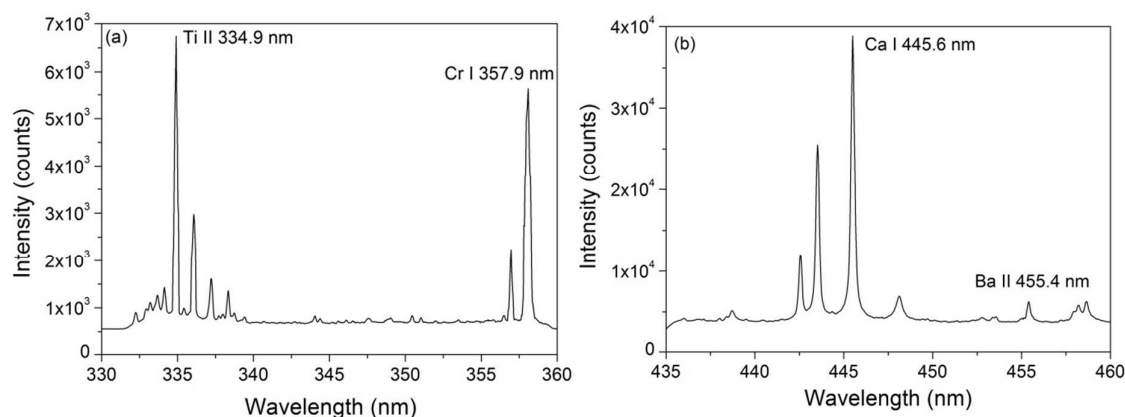


Fig. 2 Emission spectra of a bottle fragment (BG3) over the two selected spectral ranges showing the lines selected for calculating the concentrations of the 4 elements of interest.

3. Results and discussions

3.1. Quantitative analysis of the fused beads

3.1.1. Calibration curves, R^2 , LoD and repeatability. The calibration curves for the 4 elements of interest established with the fused beads are shown in Fig. 3. Each data point in the figure represents the mean intensity of the 100 replicates and the associated error bar the standard deviation, $\pm\sigma_I$, of the intensity. In the same figures, linear regressions obtained with the least-square method (LSM) of the experimental data are also shown.¹⁸

$$y = a + s \cdot x \quad (1),$$

where y is the intensity of the emission line chosen for an element of interest, x its concentration determined with XRF, s the slope of the calibration curve and a the intercept. The fitting parameters of the calibration curves for the 4 elements are shown in Table 2. We can see excellent correlation between the experimental data and the linear regression, since all the determination coefficients, R^2 , obtained from the fitting are higher than 0.999. The limit of detection (LoD) for each element is determined according to the following definition:

$$LoD = 3 \sigma_B / s \quad (2),$$

where σ_B is the standard deviation of the background of the averaged spectrum taken nearby the emission line and s the slope of the calibration curve. The values of σ_B and LoD determined for the 4 elements are shown in Table 2. The LoDs determined with LIBS are further compared to those obtained with XRF. We can see that similar LoDs are found for the 2 techniques, except for Ca.

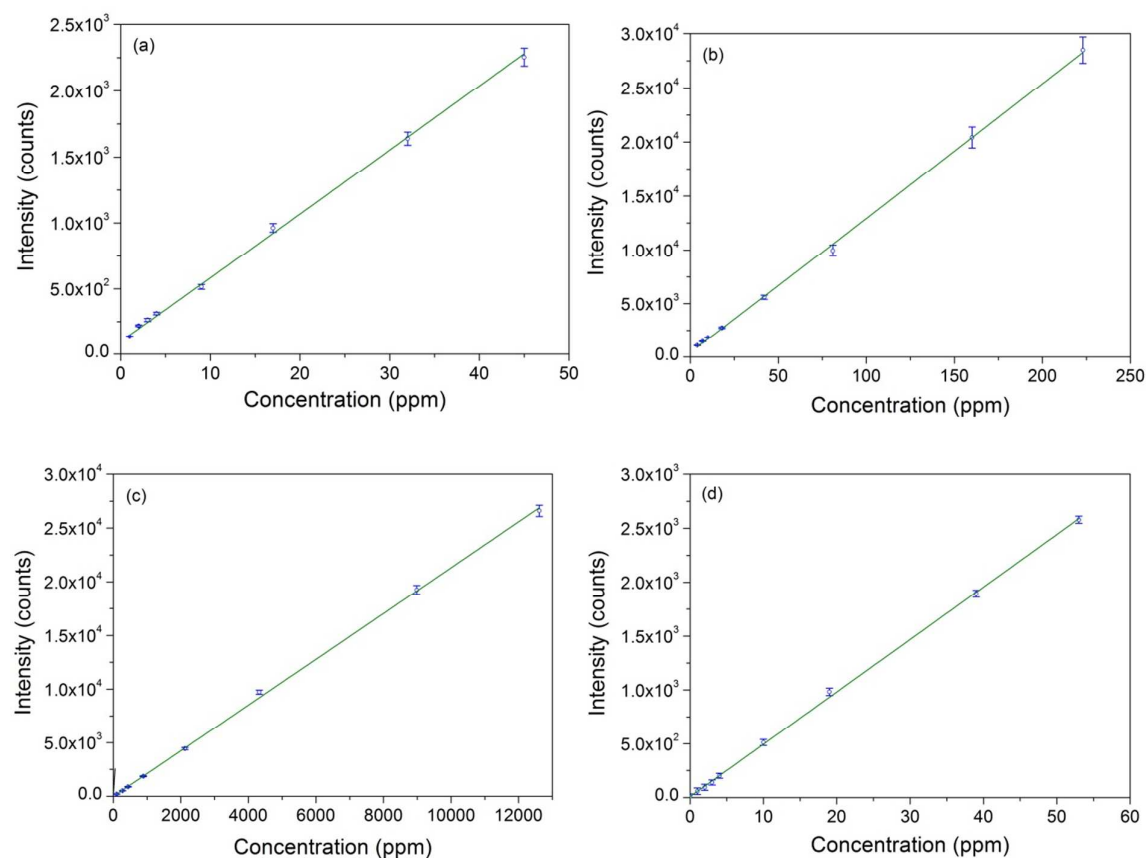


Fig. 3 Calibration curves obtained for the 4 elements of interest with the fused beads, (a) Ti, (b) Cr, (c) Ca and (d) Ba. The concentrations are those determined by XRF.

Table 2 Fitting parameters of the calibration curves, background standard deviations, σ_B , and the LoDs for the 4 elements of interest. LoDs with XRF are also provided for comparison.

Elements	Slope s	Intercept a	R^2	σ_B	LoD (ppm)	LoD XRF (ppm)
Ti	47.8	113	0.99994	9.39	0.59	0.20
Cr	123	594	0.99991	28.8	0.71	0.60
Ca	2.11	-19.9	0.99983	1.61	2.29	0.10
Ba	49.0	7.00	0.99987	11.4	0.70	0.10

1
2
3
4
5
6
7
8
9
10
11
12
13
14
15
16
17
18
19
20
21
22
23
24
25
26
27
28
29
30
31
32
33
34
35
36
37
38
39
40
41
42
43
44
45
46
47
48
49
50
51
52
53
54
55
56
57
58
59
60

The results show thus sub-ppm LoDs for the three trace elements Ti, Cr, and Ba. Such level of sensibility is comparable to that offered by XRF as we can see in Table 2. For Ca, the concentration range between 100 and 12000 ppm was not appropriate for the determination of the LoD. In spite of this issue, we were still able to determine a LoD of 2.3 ppm, illustrating the large linear dynamic range of the used setup. It is worth to point out that the analysis performed by LIBS is localized in a small point on the sample surface with typically a depth of 10 μm and a lateral dimension of 100 μm . Such spatial resolution can be an advantage if an elemental mapping^{19,20} is required on the surface of an inhomogeneous material. On the other hand, LIBS can suffer from the inhomogeneity of a sample even though sampling with ablations on a matrix of craters can be performed as it was the case in this experiment. On the contrary, XRF is suitable for sampling a larger volume of a material and measuring averaged content in the volume. Such difference underlines the specificities of each of these techniques to answer different types of applications.

We can finally see in Fig. 3 that the error bars for the 100 replicates are quite small, which can be associated to a good repeatability of the measurement. We provide the repeatability of single crater (10 laser shots) measurement in Table 3 where we define the repeatability as the percentage of the ratio $2\sigma_s/C$, with σ_s the standard deviation of the concentration deduced from the 100 replicate measurements, and C the mean concentration. We can see that for the 3 elements Ti, Cr and Ca, the reproducibility is quite good and remains always smaller than 10%. Moreover there is not a clear tendency correlated to the elemental concentration. A mean value of 5.8% is obtained when averaged over all the samples for these 3 elements. Such good repeatability shows the high stability of the used setup and the good homogeneity of the samples for these 3 elements. For Ba, the repeatability for high concentrations (> 10 ppm) is quite good similar to the other 3 elements. However for lower concentrations (< 10 ppm) the repeatability is significantly degraded. This is certainly due to the weakness of the Ba line used for its concentration determination (Fig. 2), which shows the close relation between the signal-to-noise ratio and the repeatability of the measurement. The degradation of the repeatability at low concentrations may also be due to a higher inhomogeneity in the samples of the Ba at low concentration of several ppm.

Table 3 Repeatability of single crater measurement, defined as the percentage of the ratio $2\sigma_s/C$, with σ_s the standard deviation of the 100 replicate measurements, and C the mean concentration.

Elements	Repeatability (%)									
	High concentration samples					Low concentration samples				
	FB1	FB2	FB3	FB4	Mean	FB5	FB6	FB7	FB8	Mean
Ti	6.0	6.1	6.7	7.0	6.4	6.5	8.5	5.9	5.9	6.7
Cr	8.5	9.5	10	6.8	8.7	4.8	3.0	3.3	3.6	3.7
Ca	4.0	4.3	3.8	5.1	4.3	4.9	5.3	4.4	5.0	4.9
Ba	2.6	3.3	6.9	11	5.9	23	34	60	104	56

3.1.2. Reproducibility. The reliability and the robustness of the measurement performed using the experimental setup and the protocol described in the section 2.2 have been assessed in terms of the reproducibility of the calibration curves. After a first series of measurement (set 1), a second one (set 2) was performed 3 months later in the same controllable condition and following the same experimental protocol. We specify that during the interval between the 2 series of measurements, the setup was used for many other measurements of different types of materials. Table 4 summarizes the characteristics of the calibration curves deduced from the two series of measurements and the differences (relative variations) between the two sets of calibration curves.

Table 4 Comparison between the characteristic parameters extracted from two sets of calibration curves established with two series of measurements separated by an interval of 3 months.

Parameters	Elements				
	Ti	Cr	Ca	Ba	
Slope	Set 1	47.77	121.60	2.11	48.96
	Set 2	47.10	122.54	2.19	47.88
	Δ (%)	1.4	0.74	3.8	2.2
Intercept	Set 1	112.6	594.2	-19.9	7.0
	Set 2	110.8	573.6	-21.0	7.8
	Δ (%)	1.6	3.5	5.5	11
R^2	Set 1	0.99994	0.99991	0.99983	0.99987
	Set 2	0.99992	0.99997	0.99914	0.99963
	Δ (%)	0.002	0.006	0.069	0.024
LoD (ppm)	Set 1	0.59	0.71	2.29	0.70
	Set 2	0.59	0.70	2.10	0.72
	Δ (%)	0	1.4	8.3	2.9

We can see that the two sets of calibration curves exhibit very close behaviors and that the relative variations of the characteristic parameters are limited within 3% except for Ca. Such good reproducibility shows first the homogeneity of the used reference samples. But more importantly, it demonstrates indeed the high level of instrumentation reliability of the used setup thanks to the tight controls introduced in the setup. Among them, the most crucial and useful control in the setup include that of the distance between the sample surface and the focusing lens, that of the position of the detection fiber with respect to the plasma morphology, and that of the laser pulse energy.

3.1.3. Relative accuracy. In order to evaluate the accuracy of the LIBS measurements, we used the established calibration curves (Fig. 3) to determinate the concentrations of the 4 elements of interest in the unknown samples. We specify here that the fact to use laboratory-prepared samples and to determine their concentrations with another analytical technique, leads to the relative character of the deduced accuracy of the LIBS measurement. The analyzed unknown samples included the two fused beads not used for the calibration curves (FB9 and FB10) and two bottle glass fragments chosen for their contents of the 4 elements of interest lying around the ranges covered by the calibration curves (BG2 and BG3). The same experimental conditions and measurement protocol were applied to the measurements of these

unknown samples. With the measured emission intensities, counter calibration using the calibration curves in Fig. 3 allowed retrieving the corresponding element concentration. In Fig. 4, the retrieved concentrations of the 4 elements of interest are shown. The measured concentrations are compared to those determined with XRF. The numerical values related to the results shown in Fig. 4 are presented in Table 5 for detailed assessment of the relative accuracy allowed by the LIBS measurement. In this table, the bias of a measurement is defined as the relative difference between the mean measured value and the reference value. The recovery is calculated with the ratio between the mean measured value and the reference value. And the precision is defined as the ratio between the uncertainty of the measurement, taken as 2 times of the standard deviation of the individual replicate measurements, and the mean measured value. The ensemble of these parameters provides actually an assessment of the relative accuracy of the LIBS measurement.

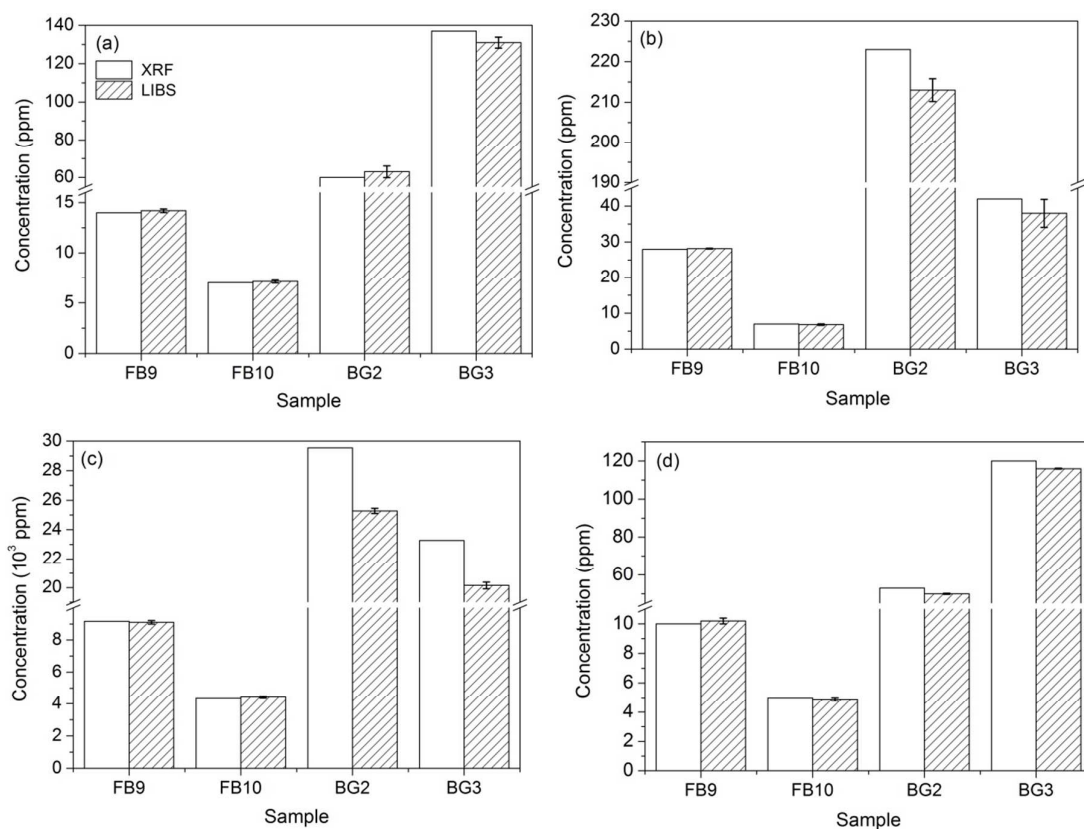


Fig. 4 Concentrations of the 4 elements of interest measured with LIBS compared to those determined by XRF (considered as reference technique) for the 4 unknown samples FB9, FB10, BG2 and BG3: (a) Ti, (b) Cr, (c) Ca and (d) Ba.

Table 5 Relative accuracy of the LIBS measurements in terms of the bias, the recovery and the precision for the determination of the concentrations of the 4 elements of interest in the 4 unknown samples.

Elements		Samples				Mean
		FB9	FB10	BG2	BG3	
Ti	Concentration (ppm)	14	7	60	137	54.5
	Bias (%)	1.4	1.4	5.0	4.4	3.1
	Recovery (%)	101	101	105	96	101
	Precision (%)	2.5	4.2	9.8	4.4	5.3
Cr	Concentration (ppm)	28	7	223	42	75
	Bias (%)	0.7	2.9	4.5	9.5	4.4
	Recovery (%)	101	97	96	91	96
	Precision (%)	0.9	6.2	2.6	21	7.5
Ca	Concentration (ppm)	9160	4319	29543	23275	16574
	Bias (%)	0.6	2.2	14	13	7.7
	Recovery	99	102	86	87	93
	Precision (%)	2.3	3.6	14	22	11
Ba	Concentration (ppm)	10	5	53	120	47
	Bias (%)	2.0	2.0	5.7	3.3	3.2
	Recovery (%)	102	98	94	97	98
	Precision (%)	3.9	4.9	12	4.0	6.3

We see in Table 5 that the bias of the determination is very small ($< 3\%$) for the 2 fused beads for all the elements analyzed. Remark that such small bias is obtained for a concentration range between several ppm to thousands ppm. The bias becomes significantly larger for the 2 bottle glass fragments. Such degradation can be due to the matrix effect between the fused beads and the collected bottle fragments and self-absorption at high concentrations (especially for Ca with a recovery $< 90\%$). But the degradation is still moderate because the worst case corresponds to a bias of 14% (Ca/BG2) and the average bias for all the elements in all the samples is 4.6%. The precision of the determination exhibits logically a better performance for the fused beads thanks to the homogeneous element distribution in these samples. It is clearly degraded for the bottle fragments. The comparison between the precisions obtained for the 2 sets of samples shows that for the setup and the experimental protocol used in this experiment, the inhomogeneity of the sample is the main reason for measurement precision degradation. Such inhomogeneity may affect both the physical properties (surface, color...) and the elemental concentration distribution inside the

1 sample. The data presented in Table 5 show moreover the precision degradation depends not
2 only on the sample but also on the element under consideration. However the overall
3 precision for all the elements in all the samples of 7.5% remains quite good.
4
5
6

7 **3.2. Quantitative analysis for bottle glass fragments**

8
9
10 In this section, we present the calibration curves established with the collected bottle glass
11 fragments. Since the concentrations of the 4 elements of interest in these samples cover a
12 much larger concentration range, the new calibration curves permit extending the
13 determination of the concentrations from the ppm level up to the percent level. Such high
14 concentration level can lead to optical thick plasma and some self-absorption on the selected
15 lines. Curvature of the calibration curves can be expected, which needs quadratic regression to
16 take into account all the data. On the other hand, the differences in matrix among the glass
17 fragments and between the glass fragments and the fused beads should lead to the matrix
18 effect. By comparing the data obtained with the glass fragments and those with the fused
19 beads, we would be able to evaluate such effects.
20
21
22
23
24
25

26 In Fig. 5, the intensities measured from glass fragments are plotted together with those
27 measured from the fused beads as a function of the concentration determined with XRF for
28 the 4 elements of interest. We can see that at low concentrations (insets in Fig. 5), these 2
29 groups of data are quite well superimposed. At high concentrations however the 2 groups
30 separate. Especially the data from glass fragments deviate from the straight line and bend into
31 a curve. As shown in Fig. 5 by solid curves, quadratic regression was thus used to fit the
32 concatenated data between the bottle glass and the fused beads
33
34
35
36
37

$$38 \quad y = a + b_1 \cdot x + b_2 \cdot x^2 \quad (3),$$

39
40 where b_1 is the linear slope, b_2 is the coefficient of the quadratic term and a intercept. The
41 fitting parameters are presented in Table 6. We can see a good correlation of the concatenated
42 data to the quadratic regression with $R^2 > 0.998$ for all the elements. Such good correlation
43 means a moderate matrix effect among the glass fragments with respect to the fused beads. It
44 shows also the fact that the saturation of the calibration curves due to multiple effects of, for
45 example, self-absorption or instrumental saturation, can be satisfactorily taken in to account
46 by quadratic regression, which represents a pragmatic way to extend the initially linear
47 calibration curve to a much more extended concentration range. This is further confirmed by
48 the fact that the linear slopes b_1 in Table 6 are quite close to the slopes shown in Table 2 and
49 the coefficients of the quadratic term remain very small compared to the corresponding linear
50 slopes. Insets are used in Fig. 5 to see in more detail, the behaviors of the data points at low
51
52
53
54
55
56
57
58
59
60

concentrations. In the same insets, we plot also the linear regressions of the data measured from the beads to show the departure of the quadratic regressions with respect to the linear ones at low concentration.

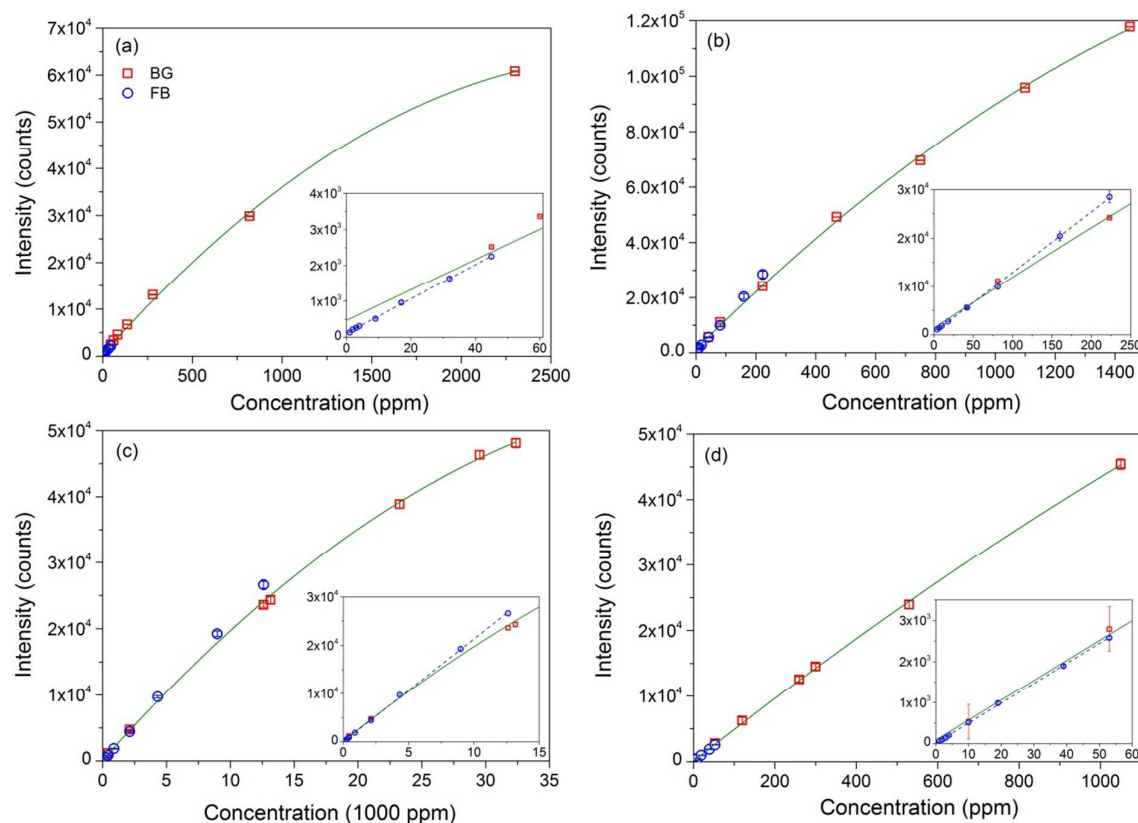


Fig. 5 Intensities measured for the 4 elements of interest in the bottle glass fragments (red squares), and in the fused beads (blue circles) as a function of the respective concentrations determined with XRF. Quadratic regressions of the ensemble of intensities (including those for fused beads and bottle glasses) are plotted for the 4 elements respectively (green curves). Insets show details at low concentrations. Linear regressions of the intensities measured in fused beads are plotted in the insets in dashed blue lines. (a) Ti, (b) Cr, (c) Ca and (d) Ba.

Table 6 Fitting parameters and determination coefficients with quadratic regression for the concatenated data between the glass fragments and the fused beads.

Elements	b_1	b_2	Intercept a	R^2
Ti	42.6	-7.2×10^{-3}	469	0.9989
Cr	108	-1.9×10^{-2}	1363	0.9991
Ca	2.17	-2.1×10^{-5}	131	0.9990
Ba	48.9	-5.5×10^{-3}	81	0.9997

4. Conclusion

In this work, the analytical figures of merit of LIBS for quantitative analysis of metallic elements in glass have been assessed with respect to XRF, a better established analytical technique. In particular, we investigated some key parameters characterizing an analytical technique, such as correlation to a linear or quadratic regression, limit of detection, repeatability, reproducibility, accuracy and ability to cover a large concentration range. The ensemble of the results obtained in this work using the developed setup and the introduced experimental protocol shows good performance, which is already comparable to those offered by XRF for elemental analysis of glass. This demonstrates indeed the current maturity of LIBS of becoming an established analytical technique. Beyond such observation, the specific capabilities of LIBS for direct analysis without sample preparation, for quick response, for high space resolution, and for addressing light elements as well as heavy ones, would make it advantageous for a large range of applications. Moreover the good performance demonstrated in this work underline the importance for a LIBS instrument to have a high degree of control and automation. This remark is particularly relevant because of the extreme sensitivity of laser-induced plasma to the ensemble of experimental conditions. We remark finally that all the analytical results shown in this paper are obtained without any normalization of the measured emission intensities. Different signal normalization procedures²¹ should improve furthermore through data treatment, the quality of the analytical results.

Acknowledgements

The authors would like to thank ANRT (Association Nationale de la Recherche et de la Technologie) and Lyon Science Transfert (LST) for their supports. They thank also the French Alsace Region for their supports.

References

1. See for example <http://glassproperties.com/glasses/>
2. See for example <http://www.infoplease.com/encyclopedia/society/glass-composition-properties-glass.html>
3. S. Klein, T. Stratoudaki, V. Zafirooulos, J. Hildenhagen, K. Dickmann, Th. Lehmkuh, *Appl. Phys.*, 1999, **A 69**, 441–444.
4. N. Carmona, M. Oujja, E. Rebollar, H. Römich, M. Castillejo, *Spectrochim. Acta, Part B*, 2005, **60**, 1155 – 1162.

- 1
 - 2
 - 3
 - 4
 - 5
 - 6
 - 7
 - 8
 - 9
 - 10
 - 11
 - 12
 - 13
 - 14
 - 15
 - 16
 - 17
 - 18
 - 19
 - 20
 - 21
 - 22
 - 23
 - 24
 - 25
 - 26
 - 27
 - 28
 - 29
 - 30
 - 31
 - 32
 - 33
 - 34
 - 35
 - 36
 - 37
 - 38
 - 39
 - 40
 - 41
 - 42
 - 43
 - 44
 - 45
 - 46
 - 47
 - 48
 - 49
 - 50
 - 51
 - 52
 - 53
 - 54
 - 55
 - 56
 - 57
 - 58
 - 59
 - 60
5. N. Carmona, M. Oujja, S. Gaspard, M. García-Heras, M.A. Villegas, M. Castillejo, *Spectrochim. Acta, Part B*, 2007, **62**, 94–100.
6. A. Giakoumaki, K. Melessanaki, Demetrios Anglos, *Anal. Bioanal. Chem.*, 2007, **387**, 749–760.
7. K. Müller, H. Stege, *Archaeometry*, 2003, **45**, 421–433.
8. X. C. Wang, V. Motto-Ros, G. Panczer, D. De Ligny, J. Yu, J. M. Benoit, J. L. Dussossoy, S. Peuget, *Spectrochim. Acta, Part B*, 2013, **87**, 139 – 146.
9. J. R. Almirall, T. Trejos, *Forensic Science Review*, 2006, **18**, 74–95.
10. C. M. Bridge, J. Powell, K.L. Steele, M. E. Sigman, *Spectrochim. Acta, Part B*, 2007, **62**, 1419–1425.
11. E. M. Rodriguez-Celis, I. B. Gornushkin, U. M. Heitmann, J. R. Almirall, B. W. Smith, J. D. Winefordner, N. Omenetto, *Anal Bioanal Chem.*, 2008, **391**, 1961–1968.
12. C. Barnett, E. Cahoon, J. R. Almirall, *Spectrochim. Acta, Part B*, 2008, **63**, 1016–1023.
13. B.E. Naes, S. Umpierrez, S. Ryland, C. Barnett, J.R. Almirall, *Spectrochim. Acta, Part B*, 2008, **63**, 1045–1050.
14. A. Ciucci, M. Corsi, V. Palleschi, S. Rastelli, A. Salvetti, E. Tognoni, *Appl. Spectrosc.* 1999, **53**, 960–964.
15. C. Gerhard, J. Hermann, L. Mercadier, L. Loewenthal, E. Axente, C.R. Luculescu, T. Sarnet, M. Sentis, W. Viöl, *Spectrochim. Acta, Part B*, 2014, **101**, 32–45.
16. V. Motto-Ros, E. Negre, F. Pelascini, G. Panczer and J. Yu, *Spectrochim. Acta, Part B*, 2013, **92**, 60–69.
17. http://physics.nist.gov/PhysRefData/ASD/lines_form.html
18. J.M. Mermet, *Spectrochim. Acta, Part B*, 2010, **65**, 509–523.
19. Q. L. Ma, V. Motto-Ros, W. Q. Lei, M. Boueri, L. J. Zheng, H. P. Zeng, M. Bar-Matthews, A. Ayalon, G. Panczer, and J. Yu, *Spectrochim. Acta, Part B*, 2010, **65**, 707–714.
20. V. Motto-Ros, L. Sancey, Q. L. Ma, F. Lux, X. S. Bai, X. C. Wang, Jin Yu, G. Panczer and O. Tillement, *Appl. Phys. Lett.*, 2012, **101**, 223702.
21. L. Li, Z. Wang, Z. Li, W. Ni, *J. Anal. At. Spectrom.*, 2011, **26**, 2274 – 2280.